Model of rhythmic ball bouncing using a visually controlled neural oscillator

Guillaume Avrin, Isabelle Anne Siegler, Maria Makarov, Pedro Rodriguez-Ayerbe

Model of Rhythmic Ball Bouncing Using a Visually Controlled Neural Oscillator

Guillaume Avrin[1,2,3], Isabelle A. Siegler[2,3], Maria Makarov[1], Pedro Rodriguez-Ayerbe[1]

[1] *Laboratoire des Signaux et Systèmes (L2S), CentraleSupélec - CNRS - Univ. Paris-Sud, Université Paris-Saclay, F-91192 Gif-sur-Yvette France*

[2] *CIAMS, Univ. Paris-Sud, Université Paris-Saclay, 91405 Orsay, France*

[3] *CIAMS, Université d'Orléans, 45067 Orléans, France*

{*guillaume.avrin*}*@u-psud.fr*

Running title: Model of Rhythmic Ball Bouncing Using a Neural Oscillator

Corresponding Author: Guillaume Avrin, UR CIAMS (EA 4532), Univ. Paris-Sud, 91405 Orsay Cedex, France (e-mail: guillaume.avrin@u-psud.fr)

Abstract

The present paper investigates the sensory-driven modulations of Central Pattern Generators dynamics that can be expected to reproduce human behavior during rhythmic hybrid tasks. We propose a theoretical model of human sensorimotor behavior able to account for the observed data from the ball-bouncing task. The novel control architecture is composed of a Matsuoka neural oscillator coupled with the environment through visual sensory feedback. The architecture's ability to reproduce human-like performance during the ball-bouncing task in the presence of perturbations is quantified by comparison of simulated and recorded trials. The results suggest that human visual control of the task is achieved on-line. The adaptive behavior is made possible by a parametric and state control of the limit cycle emerging from the interaction of the rhythmic pattern generator, the musculoskeletal system and the environment.

Ball bouncing; Information-movement couplings; Behavioral modeling; Visual control; Neural oscillators

New & Noteworthy

The study demonstrates that a behavioral model based on a neural oscillator controlled by visual information is able to accurately reproduce human modulations in a motor action with respect to sensory information during the rhythmic ball-bouncing task. The model attractor dynamics emerging from the interaction between the neuromusculoskeletal system and the environment met task requirements, environmental constraints and human behavioral choices without relying on movement planning and explicit internal models of the environment.

Introduction

A successful interaction between the central nervous system, the musculoskeletal system and the environment is crucial to behave efficiently in a dynamic environment (Beer 2009). The study of rhythmic movements in vertebrates allows for a better understanding of these interactions and associated control strategies. Several electrophysiology-based studies show that some rhythmic movements are the result of spinal cord control units activating muscle synergies based on an efficient sensorimotor integration. In particular, it has been shown that rhythm generators, known as Central Pattern Generators (CPGs), are present at the spinal level in vertebrates to produce basic rhythmic movement patterns such as locomotion and respiration (Grillner 2006; Zehr et al. 2004). The dynamics of CPGs are modulated by sensory signals through low-level information-movement couplings (Pearson 2004), and descending signals from the cerebrum (Grillner 2006; Harris-Warrick 2011; Rossignol et al. 2006). However, the neural basis of the control architectures and the sensorimotor couplings generating rhythmic movements remains unclear. Specifically, the way the Central Nervous System (CNS) might achieve the observed robust and efficient visual control of actions during cyclic hybrid tasks, such as walking or bouncing a ball, is still under investigation (Ankarali et al. 2014; Ronsse et al. 2010; Wei et al. 2007).

Based on recent experimental results involving object catching, hitting or locomotion, Zhao and Warren (2015) suggested that human action is controlled on-line, without relying on internal models of the environment, when current visual information is available. According to this study, the alternative model-based control strategy, with action guided by an internal representation

of the world and musculoskeletal system, was shown to be better suited to visually-directed actions such as during tasks where participants are first allowed to memorize the environment and then move in it blindfolded.

Among the competing approaches to the on-line visual control of action, the information processing theory considers that during limb synchronization with external periodic signals, movement characteristics such as period or phase are corrected on a cycle-to-cycle basis, through sequential auto-regressive relations called *intermittent couplings* (Van Der Steen and Keller 2013). However, as several studies show that during synchronization tasks the human neural system relies on dynamic phenomena such as entrainment and resonance tuning, the dynamic systems theory considers that synchronization is a result of these phenomena originating from the continuous coupling of the CPG with other oscillators from the neuromusculoskeletal system or from the environment (Van Der Steen and Keller 2013; Warren 2006). Visuomotor resonance tuning and entrainment phenomena, also called *global entrainments* in the literature (Taga 1995), have been observed during locomotion (Pelah et al. 2015), postural sway (Bertenthal et al. 1997), synchronization of the human arm oscillation with an oscillating external event (Schmidt et al. 2007), interpersonal visual coordination of limb oscillations (Oullier et al. 2008; Schmidt et al. 1998) and visuomotor tracking of a sinusoidally moving target (Wimmers et al. 1992). Recent results even suggest that they could emerge without conscious awareness of the visual stimuli, as the visuomotor coupling would be based on the neural pathways from retina to Area V5/MT that by-pass Area V1 (Pelah et al. 2015).

To contribute to the debate opposing these theories, the present paper considers the one-dimensional (vertical) ball-bouncing task. It is a well-known model system in neuroscience (Ankarali et al. 2014; Bazile et al. 2013, 2016; Marchal-Crespo et al. 2015; Morice et al. 2007; Ronsse et al. 2010; Ronsse and Sternad 2010; Schaal et al. 1996; Siegler et al. 2010, 2013; Sternad et al. 2001; Wei et al. 2007, 2008), robotics (Buehler et al. 1994; Kulchenko and Todorov 2011; Williamson 1999) and nonlinear dynamics (Vincent and Mees 2000) to investigate control and stability of tasks involving an agent coupled with an environment through contacts and information exchanges. The agent oscillates the paddle to hit the ball in such a way that the ball ideally reaches a predefined target height at each cycle (see Fig. 1). Imposing a target height allows for analysis of the processes involved in error-to-target correction in addition to ball-paddle timing synchronization.

Different models of paddle juggling have been proposed to analyze the information-movement couplings involved during human ball bouncing, including open-loop control models (Dijkstra et al. 2004; Schaal et al. 1996; Wei et al. 2007, 2008), optimal control models (Marchal-Crespo et al. 2015; Kulchenko and Todorov 2011; Ronsse et al. 2010; Ronsse and Sternad 2010) and Matsuoka oscillator-based models (de Rugy et al. 2003; Williamson 1999). As this the ball-bouncing task exhibits a dynamically stable regime where small perturbations of the bounce die out without requiring active control (Dijkstra et al. 2004; Schaal et al. 1996), the open-loop models generally attempt to quantify how much passive control of ball bouncing would explain the observed performances during the task performed by humans. It has recently been shown that active control strategies were also involved during the task (Ankarali et al. 2014; Wei et al. 2007, 2008). Optimal controllers have efficiently reproduced the discrete, low frequency paddle movements observed in human ball bouncing for small gravity acceleration values (between 0.61 and $9.81 m.s^{-2}$) (Marchal-Crespo et al. 2015; Ronsse et al. 2010; Ronsse and Sternad 2010). For higher frequency movements (because of higher gravity value or lower target height), human arm trajectories are rhythmical and almost sinusoidal. To generate the almost sinusoidal paddle trajectories observed during rhythmic ball bouncing, de Rugy et al. (2003) made the interesting assumption

that a CPG, modeled by a Matsuoka oscillator, generates paddle oscillations. The robustness to perturbation of these active control strategies is made possible by the use of the environment condition values, defined by the gravity acceleration g and the ball-paddle restitution coefficient α. It would be interesting to analyze whether a parsimonious model of ball bouncing necessarily has to dispose of these values in order to reproduce the observed behavior.

Assuming that rhythmic movement control relies on low-level and oscillatory CPGs, the present study evaluates the hypothesis that rhythmic movements of experienced participants are organized by sensory information through continuous information-movement couplings between the ball and paddle trajectories during rhythmic ball bouncing (for gravity acceleration higher than 6 $m.s^{-2}$ and target height lower than 1 m). According to this hypothesis the phase and frequency locking phenomenon emerging from this coupling would preclude the need for quantitative values of the environmental conditions or any explicit internal model of the environment, trajectory planning and on-line optimization.

To test this hypothesis, the present study proposes a human ball bouncing model implementing a CPG model continuously coupled to the ball trajectory to ensure synchronization between the paddle and the ball. Moreover, a parametric controller scales the CPG dynamics to cancel bounce errors and address perturbations, as in Avrin et al. (2016); de Rugy et al. (2003). Both control processes are based on visual information only. The Matsuoka oscillator was chosen from existing CPG models as it constitutes a parsimonious half-center structure already attested to model rhythmic movement generation in human ball-bouncing (de Rugy et al. 2003), biped walking (Taga 1995) and tremor modeling (Zhang et al. 2009). This model respects as much as possible the known results concerning the actual neural architecture involved in the control of rhythmic movements. It presents supraspinal control signals that scale the movement based on information from the target in Cartesian space (i.e. bounce error). The paddle trajectory (velocity and acceleration profiles) is encoded on the CPG attractor dynamics whose outputs can be viewed as motor primitives (Degallier et al. 2011; Hogan and Sternad 2012). During the movement, CPG motor primitives are modulated by sensory feedback, that takes the form of information-movement couplings, in order to adapt the movement to an unknown or changing environment (Siegler et al. 2010; Warren 2006).

To summarize, human visual control of rhythmic action is investigated in the present study by comparing human performance acquired by a virtual-reality setup with a behavioral model. It provides insight into how neural system internal dynamics are related to sensory information and adapted to palliate perturbations in a changing environment. The results support the hypothesis that human behavior during ball bouncing is controlled on-line based on visual information. Section 1 presents the experimental data that raise a number of questions about human motor control of ball bouncing and requiring further investigation. Then, a candidate CPG-based control architecture, a parameters setting method and a validation method are proposed. The results are presented in Section 2 and discussed in Section 3.

1 Methods

1.1 Human control of ball-bouncing

1.1.1 Experimental data used for analysis

General experiment information In the considered ball-bouncing task, the agent handles a paddle and moves his/her arm (movement approximated by a rotation at the elbow) to bounce a ball vertically. At each cycle, the ball's apex must be as close as possible to a predefined target height h_p. The article uses the following notations (Fig. 1): θ is the angle between the horizontal axis and the forearm, $T_b(k)$ is the ball trajectory period during cycle k, i.e. between impact k and impact $k+1$. $T_r(k)$, and $\varepsilon(k)$ are the paddle period and the bounce error of cycle k. Bounce error is defined by the distance between the ball apex $h_a(k)$ and the target height h_p ($\varepsilon(k) = h_a(k) - h_p$).

The experimental data used in the present paper were acquired during the two experiments presented in Siegler et al. (2010), where 13 experienced participants freely moved a real table tennis paddle with their preferred hand in 3-D. The vertical component of this movement was used to move a virtual paddle vertically, to hit a ball in a virtual environment. The paddle trajectories were recorded by an electromagnetic sensor (Flock of Bird Model 6DFOB ©, Ascension Technologies, with a sampling rate of 120 Hz) attached on the back side of the paddle, at $0.2\,m$ from the tip. The sensor was connected to an electromagnetic transmitter via a flexible, lightweight cable, long enough to not interfere with the participants' movements. The latency between the real and virtual paddles was equal to $29.78 \pm 1.07\,ms$ (See Morice et al. (2008) for a complete description of the experimental setup).

[FIG. 1 about here.]

The 1-D, single-joint movement hypothesis Previous studies modeling the information-movement couplings involved during human ball bouncing hypothesized that the rhythmic arm movement could be approximated by a 1-D single-joint movement at the elbow reproducing, in first approximation, the combined movement resulting from possible oscillations at the shoulder, elbow and wrist (Kulchenko and Todorov 2011; de Rugy et al. 2003; Ronsse et al. 2010; Ronsse and Sternad 2010; Schaal 2006; Williamson 1999). This common assumption facilitates comparison between the different modeling approaches. It is also considered in the present study (see Figure 1).

The legitimacy of the 1-D single-joint approximation first relies on *kinematics* considerations. During the experiments presented in Siegler et al. (2010), the participants were asked to use only rotations at the elbow to move the paddle. They were more specifically asked to not move their wrist and to keep their arm aligned with their thorax, thus avoiding shoulder movements. If, for example, residual rotations at the wrist were present in addition to the rotations at the elbow, then the two joints' oscillation frequencies should have been equal to efficiently achieve the ball bouncing task. As the angular displacements were small during the task (Ronsse et al. 2010) because of the chosen target height ($h_p = 0.80\,m$ in Ronsse et al. (2010) and $0.55\,m$ here), the paddle trajectory could be linearized and approximated by a single-degree of freedom rotation at the elbow. In Ronsse et al. (2010), the authors showed that mean human paddle trajectory was accurately reproduced by a 1-D single-joint biomechanical model.

Secondly, the legitimacy of the 1-D single-joint hypothesis relies on *performance-related* considerations. To attest that constraints on wrist movement do not modify bouncing precision, the present study analyzed the influence of constrained wrist movements on the participants' mean bounce error and standard bounce error during ball bouncing. A group of 11 participants performed ball bouncing trials under two different conditions using the virtual reality set-up presented in Morice et al. (2008) and used in Siegler et al. (2010). One condition consisted in performing the task with unconstrained wrist movements and the second with wrist movements constrained by a rigid splint. At the beginning of the experiment, each participant performed nine

familiarization trials for each wrist condition. The target height h_p was taken among three different values ($0.55,\ 0.70,\ 0.85\,m$) and changed every three familiarization trials. Then, the participants performed three trials for $h_p = 0.70\,m$ and for each of the constraint conditions presented in randomized order. Each trials lasted $45\,s$ and the environmental conditions were $g = 9.81\,m.s^{-2}$, $\alpha = 0.48$. Mean bounce error was equal to $0.022 \pm 0.07\,m$ for the unconstrained group and $0.015 \pm 0.07\,m$ for the constrained group, inducing no significant difference between the groups ($p = 0.52$). Mean bounce error standard deviation was equal to $0.141 \pm 0.056\,m$ for the unconstrained group and $0.129 \pm 0.047\,m$ for the constrained group, inducing no significant difference between the groups ($p = 0.27$). In addition, as in Sternad et al. (2001), no significant influence of the constrained wrist movement on the paddle acceleration at impact was observed. These results therefore support the present study 1-D single joint hypothesis.

Perturbed human ball-bouncing trials In Experiment 2 of Siegler et al. (2010), an environmental parameter (g or α) was suddenly changed during ongoing bouncing. The experiment was performed by 13 participants, each participant performing 12 trials with three perturbations (either on g in Session G, or on α in Session A) separated by 12 or 16 seconds. In Session G, the g was changed at the ball apex. In Session A, α was changed just before impact. The 16 perturbation conditions tested are recalled in Table 1. In the present paper, these perturbation conditions are separated into *behavior tuning* conditions used to set the model parameters presented in the next Section, and *behavior validation* conditions used for model validation. This separation of the perturbation conditions is used to test model predictive capacity and to avoid overfitting. It has been achieved so that each group of conditions includes each environment condition, the same number of high and small perturbation magnitudes and the same number of decreases and increases of the environment parameter. As in Wei et al. (2007) and Siegler et al. (2013), Siegler et al. (2010) showed an active control of paddle oscillation, even during steady-state bouncing in the passively stable region. Paddle movement adjustments occurred for both small and large perturbations, and were proportional to the perturbation magnitude. The participants were able to independently control the paddle oscillation period and magnitude to stabilize bouncing. Investigating which visual information participants used to adapt the paddle period, Siegler et al. (2010) concluded that the value of g is not information that is likely to be used (if known) by participants to control paddle trajectory. Firstly, they showed that the paddle period poorly correlates with ball velocity after impact, that could be used to determine the ball period if participants knew the value of g, and better correlated with the upward ball period. Siegler et al. (2013) reached the same conclusion based on more recent results. Secondly, the adjustments of the paddle period were rapid after a perturbation on g (within one cycle). On average, perturbation on g recovered after two cycles and perturbation on α after three cycles. These rapid adaptations do not likely allow sufficient time to learn a new value of g. In addition, gravity acceleration was changed in the virtual environment but not in the real world. Thus, the perturbations directly affected ball dynamics but arm dynamics were still subjected to normal gravity acceleration on Earth. A motor control strategy relying on an explicit knowledge and estimation of g would suppose that participants are able to attribute the perturbation to a modification of g, but also to realize that only gravity in the virtual environment has been changed but not the one on Earth. This uncommon situation should be difficult to manage for control strategy based on an explicit internal representation of the gravity. In contrast, humans were able to robustly and quickly react to these perturbations.

Siegler et al. (2010) also observed that the adaptation of the paddle period was rapid whereas the paddle amplitude shifted gradually after a perturbation. These differences may indicate the existence of two different control strategies. Recent results from Siegler et al. (2013) revealed that during human ball bouncing, control of paddle trajectory is achieved visually, on a cycle-by-cycle basis. During each cycle, the period of the paddle oscillation T_r is modulated to match the period of the ball T_b, and the paddle velocity from the previous impact is adapted proportionally to bounce error ε. The relations summarizing these results, collected in the paper under the term *information-movement couplings*, are:

$$\begin{aligned} T_r(k+1) &= \Lambda_{per} T_b(k+1) \\ \Delta V_r(k+1) &\widehat{=} V_r(k+1) - V_r(k) = \Lambda_{vel}\varepsilon(k) \end{aligned} \tag{1}$$

with Λ_{per} a constant ($\Lambda_{per} \approx 1$), Λ_{vel} a negative constant and $V_r(k)$ the paddle velocity at impact k. In the virtual environment, the ball is considered to be mass-free. Paddle velocity is unaffected by impact with the ball, and paddle velocity just before impact is equal to paddle velocity just after impact. The present paper also evidenced similar information-movement couplings for the perturbed trials of Siegler et al. (2010). An example of perturbed trial ($g = 9.81 \rightarrow 13.69,\ \alpha = 0.48$) from a representative participant of Experiment 2 of Siegler et al. (2010) is presented in Fig. 2.

[FIG. 2 about here.]

Table 1. Experimental data from Siegler et al. (2010) used for tuning and validation

Exp. #	Session A ($g = 9.81$)	Session G ($\alpha = 0.48$)	# conditions	Use in the present study
1	Steady-state	Steady state	9	Noises strengths tuning
	$\alpha \in \{0.55, 0.52, 0.48, 0.45, 0.41\}$	$g \in \{6.56, 8.10, 9.81, 11.66, 13.69\}$		
2	Perturb. on α	Perturb. on g	8	Behavior tuning
	$\alpha = 0.48 \rightarrow 0.55$	$g = 9.81 \rightarrow 6.56$		
	$\alpha = 0.45 \rightarrow 0.48$	$g = 11.66 \rightarrow 9.81$		
	$\alpha = 0.48 \rightarrow 0.41$	$g = 9.81 \rightarrow 13.69$		
	$\alpha = 0.52 \rightarrow 0.48$	$g = 8.10 \rightarrow 9.81$		
2	Perturb. on α	Perturb. on g	8	Behavior validation
	$\alpha = 0.48 \rightarrow 0.52$	$g = 9.81 \rightarrow 8.10$		
	$\alpha = 0.41 \rightarrow 0.48$	$g = 13.69 \rightarrow 9.81$		
	$\alpha = 0.48 \rightarrow 0.45$	$g = 9.81 \rightarrow 11.66$		
	$\alpha = 0.55 \rightarrow 0.48$	$g = 6.56 \rightarrow 9.81$		

Steady-state human ball-bouncing trials Experiment 1 of Siegler et al. (2010) investigated steady-state performance of humans during ball bouncing. Thirteen participants performed 40 second-long trials during which environmental conditions were kept constant, but the values of α and g were changed between trials. The participants were subjected to five different environmental conditions in two different experimental sessions referred to as Session A and Session G. In Session A, α was varied (0.55, 0.52, 0.48, 0.45, 0.41, in each condition respectively), with $g = 9.81$. In Session G, g was varied (6.56, 8.10, 9.81, 11.66, 13.69 $m.s^{-2}$, in each condition respectively), with $\alpha = 0.48$. Note that one condition was the same in both sessions ($g = 9.81,\ \alpha = 0.48$). Target height h_p was 0.55 m for all trials in both experiments.

The different environmental conditions required different ball steady-state velocities after impact. To produce these velocities during Session A, the participants decreased paddle amplitude for increased values of α, while paddle period was constant.

During Session G, paddle period decreased with the increased value of g, completed with a small increase in paddle amplitude. They were able to stabilize the task for all the conditions tested.

1.1.2 Questions raised by the experimental data

The main goal of the present paper is to better understand the information-movement couplings used by participants during steady-state and transient state ball bouncing. The steady-state and perturbed trials presented above demonstrated the participants' ability to independently adapt paddle period and amplitude to control the task. Thus two independent adaptation processes have to be investigated and modeled.

A purely open-loop model relying only on passive error-correction due to the natural dynamics of the task cannot account for such observed active control and was thus discarded. Two controllers were previously proposed to model human active control of action during the ball bouncing task. Ronsse et al. (2010), Ronsse and Sternad (2010) presented an optimal controller and de Rugy et al. (2003) a CPG-based controller. The former considered both period and amplitude adaptation whereas the later considered only period adaptation. As mentioned in the Introduction, these two models efficiently reproduce some aspects of human behavior during the ball-bouncing task by implementing on-line visual control of paddle oscillation based on an explicit value of the gravity acceleration. The optimal controller proposed in Ronsse and Sternad (2010) used the values of g and α, at least at the beginning of the trial, in order to compute controller gains. The robustness of the controller to perturbation of these environmental conditions during on-going trials was not studied. The Matsuoka oscillator-based controller proposed in de Rugy et al. (2003) accurately reproduced participants' transient state bounce error series after perturbation on α thanks to active control of the paddle period. To do this, the model integrates the value of g and estimates the ball period based on the mathematical relation that exists between ball velocity after impact and ball period. The capacity of these two previously proposed controllers to robustly stabilize ball bouncing after sudden perturbations on g was not investigated.

Siegler et al. (2010) rejected the hypothesis that the gravity acceleration was used (if known) by participants during ball bouncing. Additionally, the participants reacted quickly and stabilized the bouncing accurately in fewer than four cycles after abrupt changes in the environment conditions (Siegler et al. 2010, 2013; Wei et al. 2007). This quick correction leaves very little time to estimate the perturbed environmental conditions, possibly recompute controller gains and finish bouncing stabilization. Thus, the results from Siegler et al. (2010) suggest, in agreement with recent human motor control studies (Zhao and Warren 2015), that the paddle trajectory is controlled on-line based on the available visual information. As a consequence, the present study intents to demonstrate that a humans might rely on a control strategy robust to gravity changes without needing to integrate or estimate a quantitative value of g.

In the next sections, we propose a model of human on-line visual control of ball bouncing. It constitutes a CPG-based, threshold-free and world representation-free control architecture able to reproduce the participants' average steady-state and transient-state behavior for perturbed and unperturbed trials with different values of α and g. Participants' bounce error time series, information-movement couplings (presented in Equation 1), and bounce error standard deviation will be the criteria to test the validity of the proposed model.

1.2 A candidate model for the control of rhythmic ball bouncing

1.2.1 Bouncing ball equations

Ball flight between impacts is governed by ballistic equations:

$$\left.\begin{aligned} X_b(t) &= X_b(k) + V_b(k)t - 0.5gt^2 \\ V_b(t) &= V_b(k) - gt \end{aligned}\right\} \text{for } t_k < t < t_{k+1} \tag{2}$$

with $X_b(t)$ ball position, t_k k-th impact instant, $X_b(k)$ k-th impact position and $V_b(k)$ ball velocity directly after impact k. The impact equation is $V_b(k) = -\alpha V_b(k)^- + (1+\alpha)V_r(k)$, $V_r(k)$ the paddle velocity at impact and $V_b(k)^-$ ball velocity directly before impact k.

1.2.2 Arm dynamic model

The arm movement during ball bouncing is approximated by a 1-D, single-joint movement of the forearm. Its mechanical impedance is a simplified model, linearized around the resting position $\theta = 0$, with constant coefficients as already used in Avrin et al. (2016) and de Rugy et al. (2003):

$$I\ddot{\theta} + \gamma\dot{\theta} + K\theta = h_1\zeta \tag{3}$$

with ζ elbow torque, I arm inertia, γ damping ratio, K arm stiffness and h_1 a constant multiplicative gain on torque input. As reported in Bennett et al. (1992), during cyclic tasks, the natural frequency of the human arm is adapted to match the first harmonic frequency of the task $\omega_{arm} = \sqrt{K/I} \approx \omega_{task}$. If I is constant, then humans adapt the arm stiffness K so that $\omega_{arm} \approx \omega_{task}$. Experimental trials used in this study show that the participants were able to stabilize bouncing after a perturbation with a perturbed ball period equal to $0.4\,s$, corresponding to $\omega_{task} = 2\pi/T_{task} = 15.7\,rad/s$ (Siegler et al. 2010). The model has to be fast enough to efficiently adapt to such perturbed ball period. Taking $\omega_{task} = 15.7\,rad/s$ while respecting the bound values of the mechanical parameters found in humans (Bennett et al. 1992) ($0.2 < \gamma/(2\sqrt{KI}) < 0.6$) and the inertial value used in de Rugy et al. (2003), the chosen parameter values are $K = 25\,kg \cdot m^2 \cdot s^{-2}$, $\gamma = 1.8\,kg \cdot m^2 \cdot s^{-1}$, $I = 0.1\,kg \cdot m^2$.

1.2.3 Matsuoka oscillator

The rhythmic movement is generated by the two tonically excited neurons of the Matsuoka half-centered neural oscillator (Matsuoka 2011). The two neurons in reciprocal inhibition activate the arm flexor and extensor muscles to generate torque at the elbow and move the forearm. Each neuron has its dynamics governed by two nonlinear differential equations integrating coupling terms:

$$\begin{aligned} \tau_r\dot{x}_1 &= -x_1 - \beta v_1 - \rho y_2 - h_0[m]^+ + u \\ \tau_a\dot{v}_1 &= -v_1 + y_1 \\ \tau_r\dot{x}_2 &= -x_2 - \beta v_2 - \rho y_1 - h_0[m]^- + u \\ \tau_a\dot{v}_2 &= -v_2 + y_2 \end{aligned} \tag{4}$$

The states $x_i(t)$ and $v_i(t)$ are the i-th neuron membrane potential and the self-inhibition responsible for the fatigue phenomenon. The neurons are coupled through the terms $y_i(t) = max(x_i(t), 0)$. Oscillator output is $y_{out}(t) = max(x_1(t), 0) - max(x_2(t), 0)$ and oscillator sensory input is $m(t)$ with $[m(t)]^+ = max(m(t), 0), [m(t)]^- = max(-m(t), 0)$. The parameters defining oscillator dynamics are ρ the mutual-inhibition intensity and β the self-inhibition intensity. u is the excitability determining oscillator output amplitude and h_0 is a constant gain on the input $m(t)$. τ_r and τ_a are the time constants determining the responsiveness of x_i and v_i respectively.

The Matsuoka oscillator has two operating modes. In the first, referred to as *forced-oscillation mode*, the oscillator can be entrained by an external signal or dynamic system to which it is coupled by the input m in a robust and stable way. In the second, referred to as *autonomous mode*, the oscillator autonomously produces a periodic limit cycle with a natural frequency denoted ω_n in the absence of rhythmic sensory input ($m = 0$).

In a previous work, we proposed a parameters tuning method for the oscillator autonomous mode performing the ball-bouncing task (Avrin et al. 2016), capitalizing on the Describing Function Analysis (DFA) of Matsuoka (2011). Two scaling coefficients c_1 and c_2 were introduced so that $\tau_r = T_b c_1$ and $\tau_a = T_b c_2$. The parameter K_n was defined as $K_n = (1/\rho)(c_1/c_2 + 1)$. The set of parameters $\{c_1,\ c_1/c_2,\ K_n,\ \beta\}$ were tuned based on graphical analysis methods and Particle Swarm Optimizations (PSO) during open-loop (without ball bouncing) and closed-loop (during ball bouncing) trials, to ensure an accurate setting of ω_n, high paddle trajectory harmonicity and rapid bounce convergence after perturbation. The identified trade-offs are recalled in Table 2. This method is used in the present paper for the tuning of ρ, β, c_1, c_2.

Table 2. Tuning trade-offs

	High value	Low value	
K_n	• high harmonicity • good DFA precision	• no simultaneous firing	Tuned parameters
	→ Tuning method: open-loop PSO optimization		
c_1	• high harmonicity	• high rapidity	
	→ Tuning method: closed-loop PSO optimization		
c_2	• For K_n and c_1 fixed, only one value leads to $\omega_n = 2\pi/T_b$		Dependent parameters
	→ Tuning method: graphical analysis		
ρ	• Depends of K_n, c_1 and c_2 values		
	→ Tuning method: using the equation defining K_n		
β	• Depends of K_n, c_1, c_2 and ρ		
	→ Tuning method: the DFA gives $\beta = c_1\rho(4\pi^2 c_2^2 + 1)/(c_1 + c_2)$		

1.2.4 Implementation of information-movement couplings in the model

A block diagram of the global system is presented in Fig. 3. The dotted lines represent intermittent signals, and the solid ones the continuous signals. References to the equations corresponding to each block of the neuromusculoskeletal system model are indicated on the figure. The control strategies involved in bounce error correction and ball-paddle impact timing of the model are presented below.

Bounce error correction The error-to-target correction of Equation 1 is implemented in the model via adaptation of joint torque magnitude. Once per cycle, the sensorimotor control unit adapts excitability u, using the relation $u(k+1) = \lambda\varepsilon(k)+u(k)$, to modify oscillator output amplitude (i.e. joint torque at the elbow). The adaptation occurs when bounce error is perceived, i.e. when the ball reaches its apex ($X_b(t) = h_a$). The excitability adaptation coefficient λ has a critical influence on the modeled behavior response time to perturbation. It is therefore the subject of tuning presented in Section 1.3.2.

Impact timing control Three different Matsuoka oscillator operating modes could be considered to achieve ball-paddle impact timing control: forced, mixed and autonomous oscillations modes. In the forced-oscillation mode, paddle period adaptation would result from entrainment of the oscillator by perception of ball trajectory. However, this mode is efficient only when oscillator natural frequency ω_n is close to ball frequency $2\pi/T_b$. Otherwise, oscillator output amplitude is affected by the amplitude of the input sensory signal. This is undesirable because oscillator output amplitude is supposed to be determined by excitability u, and because it was shown that paddle amplitude and period can be controlled independently by humans during the ball-bouncing task (Siegler et al. 2010).

As a consequence, using forced-oscillation mode of the oscillator also supposes that oscillator natural frequency is adapted to be equal or close to ball frequency when the difference becomes too large. If no internal model of ball ballistic flight is considered, oscillator natural frequency adaptation can only occur when the ball period is known by the participants, i.e. when the ball is at its apex ($X_b(t) = h_a$). This forced-oscillation mode with oscillator natural frequency adaptation will be refered to as *mixed-oscillation mode*.

On the contrary, autonomous mode of the oscillator, with natural frequency adaptation at the ball apex to equal ball frequency, is less robust than mixed-oscillation mode. The ability of the three modes (autonomous, forced and mixed) to stabilize bouncing for different gravity values (and $\alpha = 0.48$ fixed) have been evaluated and the results are shown in Fig. 4. It can be seen that mixed-oscillation mode was the only one to be stable for any of the tested values of g (between 5 and 12.2 $m.s^{-2}$). In addition, autonomous oscillation mode gives rise to unrealistic behaviors, as in Fig. 5. This figure presents a situation where a perturbation on a cycle leads to a ball period largely higher than the oscillator one. In this case, as the oscillator natural frequency is only modified at the ball apex, the paddle completes two cycles before reacting to the large ball period. This behavior is not observed during human ball bouncing. Rather, humans tend to react to large changes of ball period before the ball reaches its apex, as evidenced in (Siegler et al. 2010) after perturbations on g.

Thus, the mixed-oscillation mode is considered in the present paper. In order to avoid adding a supplementary threshold parameter, oscillator natural frequency adaptation is achieved on a cycle basis directly after the ball reaches its apex, via a modification of oscillator time constants τ_r and τ_a. The information-movement coupling responsible for paddle period adaptation, presented in Equation 1, is implemented in the model via a low-level coupling between perceived ball velocity and the oscillator. The continuous oscillator input m is equal to perceived ball velocity delayed by a duration t_d: $m(t) = V_b(t - t_d)$. t_d will be referred to as visual time delay in the present paper. This delay affects the ball-paddle impact phase as presented in Section 1.3.1. Therefore, it is subject to tuning presented in the same section.

To summarize, oscillator dynamics are modulated by sensory information via Equation 5.

$$\left.\begin{array}{l} u(k+1) = \lambda\varepsilon(k) + u(k) \\ \tau_r = c_1 T_b(k),\ \tau_a = c_2 T_b(k) \end{array}\right\} \text{adaptation when } X_b(t) = h_a(k)$$
$$m(t) = V_b(t - t_d) \tag{5}$$

Finally, participants exhibit variability in bounce error ε during steady-state bouncing. In the present paper, we hypothesize that two sensory noises (on ball period and ball apex perceptions) and one motor noise (affecting joint torque) cause this variability. They are considered to be additive Gaussian white noises: $\tau(t) = y_{out}(t) + S_1 W_1(t)$, $u(k+1) = u(k) + \lambda\varepsilon(k) + S_2 W_2(k)$ and $T_r(k) = T_b(k) + S_3 W_3(k)$ with W_i Gaussian white noise and S_i its strength (or standard deviation).

[FIG. 3 about here.]

[FIG. 4 about here.]

[FIG. 5 about here.]

1.2.5 Summary of tunable parameters

The proposed model contains 11 tunable parameters: $\{c_1, c_2, \rho, \beta, h_0, h_1, t_d, \lambda, S_1, S_2, S_3\}$. The parameters $\{c_1, c_2, \rho, \beta\}$ have been chosen according to the method first proposed in Avrin et al. (2016) and recalled in Section 1.2.3. Thus, we do not address their tuning further in the present study. These parameters are kept constant for all of the simulations presented in the paper.

Three parameters affect the limit cycle of the closed-loop hybrid system: visual input delay t_d of Equation 5, oscillator input gain h_0 of Equation 4 and mechanical arm input gain h_1 of Equation 3. Finally, the parameter λ influences system response time, and noise strengths S_1, S_2 and S_3 influence performance variability. Table 3 summarizes model tunable parameters.

The model parameters are tuned and validated based on simulations using Matlab/C programs with a sampling rate $t_s = 3ms$. The neural oscillator and arm differential equations are integrated numerically using Matlab *ode*23 solver.

Table 3. Tunable model parameters

Parameter	Value	Influence on the modeled motor behavior
Neurons membrane potential time constant coefficient	$c_1 = 0.137$	Intra-cycle paddle trajectories (cf. Section 1.2.3)
Neurons self-inhibition time constant coefficient	$c_2 = 0.314$	Intra-cycle paddle trajectories (cf. Section 1.2.3)
Neurons self-inhibition intensity coefficient	$\rho = 1.689$	Intra-cycle paddle trajectories (cf. Section 1.2.3)
Neurons mutual-inhibition intensity coefficient	$\beta = 2.512$	Intra-cycle paddle trajectories (cf. Section 1.2.3)
Oscillator input gain	$h_0 = 96.54$	Ball-paddle impact phase (cf. Section 2.1)
Oscillator output gain	$h_1 = 0.610$	Oscillator entrainment by input (cf. 2.1)
Oscillator visual input delay	$t_d = 36.00\,ms$	Ball-paddle impact phase (cf. Section 2.1)
Oscillator excitability adaptation coefficient	$\lambda = -3.400$	Error correction response time (cf. Section 2.1)
Noise strength on joint torque	$S_1 = 0.946$	Bounce error variability (cf. Section 2.3)
Noise strength on ball apex perception	$S_2 = 0.083$	Bounce error variability (cf. Section 2.3)
Noise strength on ball period perception	$S_3 = 0.004$	Bounce error variability (cf. Section 2.3)

1.3 Parameter influences on the modeled behavior dynamics and tuning methods

The parameters $\{t_d,\ h_0,\ h_1,\ \lambda\}$ are set so that the bounce error correction strategies implemented in the model match the human ones analyzed in Experiment 2 of Siegler et al. (2010). More specifically, the model bounce errors of the two ball cycles

before perturbations and the eight ball cycles following the perturbation are compared to human ones. The influence of these parameters on the simulated behavior is described in the following paragraphs and the tuning method is deduced.

1.3.1 Limit cycle shaping

Fig. 6 presents an example of a participant's reaction to a perturbation during the ball-bouncing task (here a perturbation on the ball-paddle restitution coefficient $\alpha = 0.41 \rightarrow 0.48$). If steady state is reached before perturbation, as is the case in the example in Fig. 6, the first two bounce errors before perturbation (steady-state errors) and the first bounce error after perturbation are unaffected by the bounce error correction strategy and so are independent of λ. As a consequence, these three bounces depend only on the characteristics of the limit cycle where the closed-loop system converged before perturbation. This limit cycle, determined by the steady-state values of the paddle position, velocity, acceleration and phase at impact (these variables being dependent of each other if the movement is considered to be almost sinusoidal) is influenced by the parameters $\{t_d,\, h_0,\, h_1\}$. For instance, the influence of t_d on the impact phase for the condition $g = 9.81, \alpha = 0.48$ is shown in Fig. 7. The higher t_d is, the lower the impact phase is, and so the sooner ball-paddle impact occurs in the cycle. The impact phase is calculated in the phase portrait, with the centered paddle position on the x-axis and the paddle velocity on the y-axis. It is equal to $360 - \phi$, with ϕ the angle at impact position. Thus, the parameter t_d could be tuned so that the paddle impacts the ball in the open-loop stable phase region (corresponding to negative paddle acceleration at impact (Schaal et al. 1996; Sternad et al. 2001)). The influence of h_1 on acceleration at impact was underlined by de Rugy et al. (2003). On the contrary, as will be shown in the next paragraph, λ influences system transient behavior and thus determines whether the system will diverge or converge towards the limit cycle defined by $\{t_d,\, h_0,\, h_1\}$.

Thus, $\{t_d,\ h_0,\ h_1,\ \lambda\}$ are tuned simultaneously by a Particle Swarm Optimization (PSO) (Yagoubi and Sandou 2011) minimizing the sum of the Mean Square Error (MSE) between the participants and model mean bounce error of the first three cycles, in the eight tuning conditions (see Fig. 6). It is important to note that with this optimization, if the bouncing steady-state is reached before perturbation (i.e. if the value of λ stabilized the system) during any simulated trial, then the cost function evaluates only the goodness of parameters $\{t_d,\, h_0,\, h_1\}$ and this cost function value is independent of the value of λ. λ is still considered as tunable in the PSO just because it is possible that some limit cycle could be reached only for specific value intervals of λ.

[FIG. 6 about here.]

[FIG. 7 about here.]

1.3.2 Transient-state shaping

The oscillator excitability adaptation coefficient λ in Equation 5 influences the information-movement coupling between bounce error ε and the change in paddle velocity at impact from previous impact ΔV_r. It acts as a negative feedback gain for bounce error correction. The more negative λ is, the lower the response time is until the point where, when decreasing too much, λ also yields an overshoot and thus reduces responsiveness. The influence of λ on response time after a target height change ($h_p : 0.55 \rightarrow 0.75m$) occurring $10\,s$ after trial initiation is illustrated in Fig. 8A. Examples with low and high absolute values

of λ, for the perturbation ($h_p : 0.55 \rightarrow 0.1m$) are given in 8B and 8C, respectively. Thus, it is possible to tune λ to match the participants' response time after perturbations. To do so, once the parameters $\{t_d,\ h_0,\ h_1\}$ were tuned using the method proposed in 1.3.1, they were kept constant and the sum of the MSE between the 13 participants and model bounce errors for the ten cycles around perturbation (two cycles before perturbation and eight cycles after perturbation) is calculated for different values of λ. The λ value leading to the minimum MSE is chosen for tuning. Note that the two cycles before perturbation will have no influence on the MSE if the considered λ value allowed the system to reach steady-state before perturbation.

[FIG. 8 about here.]

1.4 Model noise level

Noise strengths S_1, S_2 and S_3 influence bounce error variability during simulation trials and thus can be set to match the observed human variability (see Fig. 9A for an illustration of human bounce error variability during a steady-state trial). Examples of simulated trials without noise (for $S_1 = S_2 = S_3 = 0$) and with motor noise (for $S_1 = 0.946,\ S_2 = S_3 = 0$) are given in Figs. 9B and 9C.

Noise strengths are considered to be adequately tuned for a specific environmental condition when the model mean bounce error standard deviation over 13 trials is within the confidence interval (CI) of the 13 participants' bounce error standard deviations calculated based on the nine trial conditions of Experiment 1 of Siegler et al. (2010). The CIs presented in the paper are calculated based on Student t-values: $CI = \left[\bar{x} - t\frac{s}{\sqrt{n}}; \bar{x} + t\frac{s}{\sqrt{n}}\right]$ with n the number of participants in the experiment, t the Student t-values corresponding to $n-1$ degrees of freedom and $p = 0.05$. s is the corrected sample standard deviation and $\bar{x}$ the sample mean.

A PSO was performed to find the values of $\{S_1,\ S_2,\ S_3\}$ minimizing the MSE between the 13 participants' and model mean bounce error standard deviations, for the nine different conditions of Experiment 1 of Siegler et al. (2010).

[FIG. 9 about here.]

1.5 Model Validation

For each participant in Experiment 2 of Siegler et al. (2010), a regression between the informational variable T_b (ball period) and the action variable T_r (paddle period) of the ten cycles around perturbation (two cycles before and eight cycles after perturbation) of the four validation conditions of Session G presented in Table 1, was achieved (180 points per regression, 13 regressions). The mean regression slope Λ_{per} is equal to 0.999 with a standard deviation of ± 0.003, leading to the calculated CI $[0.999 - 0.002; 0.999 + 0.002]$. For the model of the human timing control of the ball-paddle impact to be validated, the model regression slope $\hat{\Lambda}_{per}$, calculated based on the simulation data vectors (T_r) and (T_b), has to be within this confidence interval, that is: $\hat{\Lambda}_{per} \in [0.997; 1.001]$.

Similarly, to characterize the human bounce error correction strategy and to serve as a reference for model validation, a regression between the informational variable ε and the action variable ΔV_r for each of the 13 participants was achieved. The trials concerned by the regression are those corresponding to the four validation conditions of Session A, presented in Table 1

(180 points per regression, 13 regressions). The mean regression slope Λ_{vel} was computed over the 13 participants in order to characterize the information-movement coupling and to serve as a reference value for model simulations. Mean Λ_{vel} is equal to -1.06 with a standard deviation ± 0.35, leading to CI $[-1.06 - 0.22; -1.06 + 0.22]$. To validate the model, the regression slope $\hat{\Lambda}_{vel}$, that is calculated based on the simulation data vectors (ΔV_r) and (ε), has to be within this confidence interval, that is: $\hat{\Lambda}_{vel} \in [-1.28; -0.84]$.

2 Results

2.1 Results of limit cycle and transient-state tuning

As presented in Fig. 10, the black dots corresponding to the different parameter values tested by the PSO algorithm converged towards the parameter set: $\{t_d = 36,\ h_0 = 96.54,\ h_1 = 0.610\}$. The cumulated MSE between the model and participants bounce error for the ten cycles around perturbation for the eight tuning conditions was then calculated for different values of λ. The value leading to the lowest MSE was $\lambda = 3.4$ (see Fig. 11). The participants and model bounce error convergences after each perturbation of the eight tuning conditions are shown in Fig. 12 for qualitative comparison. It can be seen that all the model bounce errors are inside the gray area corresponding to mean ± SD of humans.

[FIG. 10 about here.]

[FIG. 11 about here.]

[FIG. 12 about here.]

2.2 Validation of modeled behavior dynamics

The different types of environmental condition perturbations require different paddle oscillation periods and amplitudes as explained in Siegler et al. (2010). The tuned controller stabilized each of the validation perturbations recalled in Table 1 and thus proved able to adapt paddle oscillations to these perturbations. The model regression slopes characterizing the sensorimotor gains of the information-movement couplings are: $\hat{\Lambda}_{vel} = -0.96$ and $\hat{\Lambda}_{per} = 1.00$. The model sensorimotor gains $\hat{\Lambda}_{vel}$ and $\hat{\Lambda}_{vel}$ are inside the two corresponding CI calculated on humans (see Section 1.3.2). In other words, the model accurately reproduces human modulations in motor action respectively to sensory information during the task. Figure 13 shows the 13 participants' performance (mean bounce error ± SD) and the model bounce error for each validation perturbation, as a function of the cycle number. It can be seen that all of the model bounce errors are inside the gray area corresponding to mean ± SD of humans.

[FIG. 13 about here.]

2.3 Result of model noise tuning

The PSO algorithm converged toward values of noise strengths $S_1 = 0.946$, $S_2 = 0.083$ and $S_3 = 0.004$. Optimization convergence is shown in Fig. 14. The black dots indicate the tested noise strengths that were successfully faced by the control architecture. It

can be seen that the proposed model is robust and leads to stable bouncing for a large range of sensory and motor noise strengths. The noise model that best reproduces the participants' bounce error variability during the steady-state experiment of Siegler et al. (2010) is composed of significant motor noise (8%) and relatively lower sensory noises (approximately 1% for ball apex and period perception). For this noise setting, the controller stabilizes bouncing for the nine environmental conditions determined by the pairs $\{\alpha,\ g\}$ presented in Section 1.1.1. Figure 15 shows nine condition-related error bars. Each one corresponds to the CI of the 13 participants' bounce error standard deviations for a particular environmental condition determined by the pair $\{\alpha,\ g\}$. Thirteen simulations are run for each environmental condition and the mean of the 13 model bounce error standard deviations is superimposed on the corresponding participants' CI. The model mean bounce error standard deviations lies within the participants' CI for all conditions but one ($\alpha = 0.55,\ g = 9.81$).

[FIG. 14 about here.]

[FIG. 15 about here.]

2.4 Analysis of robustness to sensory information sampling

As presented in Section 1.2.4, the input of the Matsuoka oscillator is the delayed signal of the perceived ball velocity. For model tuning and validation, the sensory input signal was considered to be continuous. However, as the sampling rate at which the subject picks up information from the environment is unknown, a robustness test on its sampling is performed to evaluate the CPG's ability to be driven by a sampled input. Thus, different sampling periods were tested during trials with environmental conditions $g = 9.81,\ \alpha = 0.48$. Once the ball velocity was discretized at a specific sampling period, it was transformed into a piecewise-constant signal using a zero-order hold. An example with a sampling period equal to 60 ms is presented in Fig. 16A. Based on the simulation results (Fig. 16B), it can be seen that bounce error standard deviation increases (non-linearly) with sampling period until bouncing becomes unstable for sampling periods over 160 ms.

[FIG. 16 about here.]

3 Discussion

The present study explored how visual information might modulate CPG dynamics via information-movement couplings in human rhythmic ball bouncing. Previous experimental studies found that 1) paddle adjustments were rapid and proportional to the disturbance magnitude, 2) the paddle oscillation period was adapted to match the ball period ($T_r = \Lambda_{per} T_b$) and 3) humans used target height perception to correct bounce error by changing paddle velocity from the previous impact ($\Delta V_r = \Lambda_{vel}\varepsilon$) (Siegler et al. 2010, 2013; Wei et al. 2007, 2008).

To model these control strategies and imitate human behavior during ball bouncing with environmental conditions leading to rhythmic movements (g higher than 6 $m.s^{-2}$ and h_p lower than 1 m), an extension of the CPG-based model of de Rugy et al. (2003) was proposed in the present study. However, the model is conceived without threshold, in agreement with recent results questioning the threshold hypothesis (Siegler et al. 2010). More importantly, it integrates an innovative mixed-oscillation mode

for the Matsuoka oscillator. With this operating mode, the intrinsic dynamics of the action system (the CPG and the arm) define a limit cycle attractor that is shifted by both state and parametric control laws. State control corresponds to the forced oscillations of the CPG that is continuously fed by the visual perception of the non-sinusoidal ball trajectory. This entrainment, completed by the intermittent mechanical coupling composed of ball-paddle impacts, leads to a resonance tuning of the ball-paddle system. The resulting perception-action cycle precludes the need for explicit internal representation of environment parameters (g, α). The generated paddle movement pattern is scaled by the parametric control of CPG excitability. The resulting model respects vertebrates' motor control organization with descending signals from the cortex that modulate CPG activity (Deliagina 2008; Drew 1988). It opens new ways of explaining human behavior observed during ball bouncing. For example, most participants were seen to hit the ball in the passive stability regime, thus independently of the initial conditions (Ankarali et al. 2014; Dijkstra et al. 2004; Siegler et al. 2010, 2013; Sternad et al. 2001; Wei et al. 2007), and this attractor would be the consequence of a behavioral choice learned with practice (Wei et al. 2008). This robust convergence toward a specific limit cycle could be the result of an additional intermittent control of paddle acceleration at impact (Avrin et al. in press). The present paper demonstrated the existence of an alternative hypothesis: the limit cycle emerges from the resonance tuning of the ball-paddle system.

Studies evidencing such visual entrainment phenomena were recalled in the Introduction. The relevance of these phenomena for modeling human ball bouncing is further supported by recent results showing that humans have the ability to efficiently synchronize (or even entrain) their limb movements specifically with a virtual bouncing ball constituting a moving visual metronome (Gan et al. 2015; Iversen et al. 2015). The vision system is efficient at processing spatial information. It leads to accurate action timing when the visual stimuli contain spatiotemporal information (Hove et al. 2013). Hove et al. (2013) show that the putamen was activated during visuomotor synchronization with a continuously moving virtual bar instead of a bouncing ball, which seems to indicate rhythm detection. The superior parietal lobule, which was reported to be part of the dorsal visual system, was also activated. This result is consistent with the suggestion of Goodale and Milner (1992) and Norman (2002) that the dorsal visual system is involved in the sensorimotor transformation related to visually guided actions. Thus, the dorsal visual stream might be involved in the entrainment of the CPG by the ball trajectory during the ball bouncing task investigated in the present study.

The modeling of human movement during ball bouncing by self-organizing dynamics of a system of coupled oscillators also seems to be coherent with previously observed human behaviors during this task. It is in agreement with Morice et al. (2007) who reported the emergence of stable behavior during ball bouncing, with behavioral dynamics depending on the order parameter $\Delta\phi$, the phase shift between ball and paddle trajectory, that was exploited by participants to stabilize the behavior. Phase shift is a well-known order parameter for inter-limb coordination (Kelso et al. 2013). In addition, the dynamic approach of ball-bouncing could possibly explain the dwell-time observed in Ronsse et al. (2010) for small gravity values. Indeed, frequency generally constitutes a control parameter for systems of coupled oscillators. Its variation can typically influence the movement pattern as observed for bi-manual coordination or locomotion gaits. For ball-bouncing, frequency decreases when gravity decreases and could thus lead to such pattern transition toward non-harmonic paddle trajectories. It would be interesting to investigate this supposition further in a future study.

The presented model efficiently reproduces human information-movement couplings during the ball-bouncing task in the

presence of perturbations, which was our main focus of study. Indeed, no significant difference existed between model sensorimotor gains (Λ_{vel} and Λ_{per}) and human ones. Furthermore, none of the model bounce errors after perturbation (Fig. 12 and 13) were outside the limits defined by the standard deviation of the 13 participants' bounce errors. This qualitative comparison illustrates the human-likeness of the behavior produced by the model.

Three main ways of refining the model and possibly reducing the slight remaining discrepancy between humans and model bounce error series could be explored. First, in our model, the parameters of the adaptation laws and the mechanical arm are considered to be constant for all of the environmental conditions and all of the perturbation magnitudes. However, it is possible that humans adapt these gains when necessary. Second, muscle dynamics, possible multi-joint movements and 3-D movement excursions are not taken into account. Simulations using a more accurate musculoskeletal model could lead to a better matching. Third, paddle acceleration at impact is not actively controlled in our model, although previous studies suggested that it might be actively controlled by participants to keep the bounce in or near the passively stable region of the paddle cycle after a perturbation deviated it (Siegler et al. 2010; Sternad et al. 2001; Wei et al. 2007, 2008). The proposed model integrates a parameter t_d that defines the phase shift between ball trajectory and paddle trajectory and therefore the paddle acceleration at impact. When t_d is zero, the impact occurs at the maximum paddle position, as in the mirror algorithm (Buehler et al. 1994), and the impact phase decreases when t_d is increased. As this phase shift could result from a combination of a visual input delay constituting a physiological constant and a voluntary phase shift, the parameter t_d could be actively controlled to regulate paddle acceleration at impact during on-going trial and possibly reduce the discrepancy. Instead of ball velocity, the authors also considered ball position as potential input of the CPG. However, when coupled with this signal, the system converged toward an impact corresponding to maximum paddle velocity that is outside the cycle's passively stable region, in contradiction with observed participant behavior.

The proposed control architecture also proved able to stabilize bouncing in the presence of both motor noise and sensory noises. High motor noise and low sensory noises best reproduced human bounce error variability. For only one condition ($g = 9.81,\ \alpha = 0.55$), model bounce error standard deviation was outside the participants' confidence interval, but was still inside standard deviation limits. In future studies, the discrepancy for one of the nine environmental conditions might be canceled by defining more complex noise models, such as multiplicative noises as often used in neuroscience (Harris and Wolpert 1998). In addition, it is known from experimental ball bouncing trials, that after large perturbations, participants do not wait for the ball to reach its apex to adapt paddle period to ball period (one reason why the behavior shown in Fig. 5 is unrealistic). Contrary to what was supposed in previous modeling studies, this means that humans integrate information from the environment more frequently than just once per cycle. Thus, the present study considered that the CPG visual input signal m was continuously fed back to the CPG. However, this work also evidenced the increase of bounce error variability with the sampling period of m. This sampling rate could be partly responsible for the variability in the participants' performance. The present model predicts that environment information has to sampled at least every 160 ms to reach a stable limit cycle. To obtain better insight of the sampling rate at which humans integrate information from the environment and improve the noise model, this prediction could be compared with a future experimental ball-bouncing task with a ball trajectory visible only at an imposed specific frequency.

In summary, without using any explicit world representation, the proposed control architecture achieves the same level of

performance as humans with the same pattern of movement, including when facing perturbations on the gravity acceleration and ball-paddle restitution coefficient. The information-movement couplings integrated in the model are in agreement with recent results supporting the strong on-line approach to visual control of action. Thus, the presented control framework is well suited to understanding the emergence of action from sensorimotor couplings in humans, and modeling rhythmic movements such as those involved in the ball-bouncing task. For robotic applications, it shows that some complex hybrid tasks can be performed by robots in a model-free control framework. Future work will extend the CPG-based control architecture so that it can produce the discrete arm trajectories involved during low frequency ball bouncing. It will also include an experimental evaluation of the proposed controller for the ball-bouncing task performed by a robotic arm.

Acknowledgments

We thank William H. Warren for preliminary discussions about ball bouncing modeling.

Grants

This work was supported by the Foundation for Scientific Cooperation (FSC) Paris-Saclay Campus.

Disclosure

No conflicts of interest, financial or otherwise, are declared by the author(s).

Author contributions

G.A. prepared figures; G.A. drafted manuscript; I.A.S. performed experiments; G.A., I.A.S., M.M., P.R-A. designed model; G.A. and M.M. performed simulations; G.A., I.A.S., M.M., P.R-A. analyzed data and interpreted results of experiments; G.A., I.A.S., M.M., P.R-A. edited and revised manuscript; G.A., I.A.S., M.M., P.R-A. approved final version of manuscript.

References

Ankarali MM, Tutkun Şen H, De A, Okamura AM, Cowan NJ. Haptic feedback enhances rhythmic motor control by reducing variability, not improving convergence rate. *J Neurophysiol* 111: 1286–1299, 2014.

Avrin G, Makarov M, Rodriguez-Ayerbe P, Siegler IA. Particle swarm optimization of Matsuoka's oscillator parameters in human-like control of rhythmic movements. *Proc IEEE American Control Conf* p. 342–347, 2016.

Avrin G, Makarov M, Rodriguez-Ayerbe P, Siegler IA. Dynamic stability of repeated agent-environment interactions during the hybrid ball-bouncing task. *Proc Int Conf Informatics in Control, Automation and Robotics* , in press.

Bazile C, Benguigui N, Siegler IA. Development of information–movement couplings in a rhythmical ball-bouncing task: from space- to time-related information. *Exp Brain Res* 234: 173–183, 2016.

Bazile C, Siegler IA, Benguigui N. Major changes in a rhythmic ball-bouncing task occur at age 7 years. *PLoS ONE* 8: e74127, 2013.

Beer RD. Beyond control: The dynamics of brain-body-environment interaction in motor systems. In: *Progress in motor control*. Springer, 2009. p. 7–24.

Bennett D, Hollerbach J, Xu Y, Hunter I. Time-varying stiffness of human elbow joint during cyclic voluntary movement. *Exp Brain Res* 88: 433–442, 1992.

Bertenthal BI, Rose JL, Bai DL. Perception-action coupling in the development of visual control of posture. *Journal of Experimental Psychology Human Perception and Performance* 23: 1631–1643, 1997.

Buehler M, Koditschek DE, Kindlmann PJ. Planning and control of robotic juggling and catching tasks. *Int J Robotics Research* 13: 101–118, 1994.

de Rugy A, Wei K, Müller H, Sternad D. Actively tracking passive stability in a ball bouncing task. *Brain Res* 982: 64 – 78, 2003.

Degallier S, Righetti L, Gay S, Ijspeert A. Toward simple control for complex, autonomous robotic applications: combining discrete and rhythmic motor primitives. *Autonomous Robots* 31: 155–181, 2011.

Deliagina TG. Overview of motor systems. types of movements: Reflexes, rhythmical and voluntary movements. In: *Dynamical Systems, Wave-Based Computation and Neuro-Inspired Robots*, edited by **Arena P**. Vienna: Springer Vienna, 2008. p. 3–14.

Dijkstra T, Katsumata H, de Rugy A, Sternad D. The dialogue between data and model: passive stability and relaxation behavior in a ball-bouncing task. *Nonlinear Studies* 11: 319–344, 2004.

Drew T. Motor cortical cell discharge during voluntary gait modification. *Brain Res* 457: 181–187, 1988.

Gan L, Huang Y, Zhou L, Qian C, Wu X. Synchronization to a bouncing ball with a realistic motion trajectory. *Scientific reports* 5: 11974, 2015.

Goodale MA, Milner AD. Separate visual pathways for perception and action. *Trends in neurosciences* 15: 20–25, 1992.

Grillner S. Biological pattern generation: The cellular and computational logic of networks in motion. *Neuron* 52: 751 – 766, 2006.

Harris CM, Wolpert DM. Signal-dependent noise determines motor planning. *Nature* 394: 780–784, 1998.

Harris-Warrick RM. Neuromodulation and flexibility in central pattern generator networks. *Curr Opin Neurobiol* 21: 685 – 692, 2011. networks, circuits and computation.

Hogan N, Sternad D. Dynamic primitives of motor behavior. *Biological cybernetics* 106: 727–739, 2012.

Hove MJ, Fairhurst MT, Kotz SA, Keller PE. Synchronizing with auditory and visual rhythms: an fmri assessment of modality differences and modality appropriateness. *Neuroimage* 67: 313–321, 2013.

Iversen JR, Patel AD, Nicodemus B, Emmorey K. Synchronization to auditory and visual rhythms in hearing and deaf individuals. *Cognition* 134: 232–244, 2015.

Kelso JS, Dumas G, Tognoli E. Outline of a general theory of behavior and brain coordination. *Neural Networks* 37: 120–131, 2013.

Kulchenko P, Todorov E. First-exit model predictive control of fast discontinuous dynamics: Application to ball bouncing. *Proc IEEE Int Conf on Robotics and Automation (ICRA)* p. 2144–2151, 2011.

Marchal-Crespo L, Bannwart M, Riener R, Vallery H. The effect of haptic guidance on learning a hybrid rhythmic-discrete motor task. *IEEE Trans Haptics* 8: 222–234, 2015.

Matsuoka K. Analysis of a neural oscillator. *Biol Cybern* 104: 297–304, 2011.

Morice A, Siegler IA, Bardy B, Warren W. Action-perception patterns in virtual ball bouncing: combating system latency and tracking functional validity. *Exp Brain Res* 181: 249–265, 2007.

Morice AH, Siegler IA, Bardy BG. Action-perception patterns in virtual ball bouncing: Combating system latency and tracking functional validity. *Journal of neuroscience methods* 169: 255–266, 2008.

Norman J. Two visual systems and two theories of perception: An attempt to reconcile the constructivist and ecological approaches. *Behavioral and brain sciences* 25: 73–96, 2002.

Oullier O, De Guzman GC, Jantzen KJ, Lagarde J, Scott Kelso J. Social coordination dynamics: Measuring human bonding. *Social neuroscience* 3: 178–192, 2008.

Pearson KG. Generating the walking gait: role of sensory feedback. *Progress in brain research* 143: 123–129, 2004.

Pelah A, Barbur J, Thurrell A, Hock HS. The coupling of vision with locomotion in cortical blindness. *Vision research* 110: 286–294, 2015.

Ronsse R, Sternad D. Bouncing between model and data: stability, passivity, and optimality in hybrid dynamics. *J Mot Behav* 42: 389–399, 2010.

Ronsse R, Wei K, Sternad D. Optimal control of a hybrid rhythmic-discrete task: The bouncing ball revisited. *J Neurophysiol* 103: 2482–2493,

2010.

Rossignol S, Dubuc R, Gossard JP. Dynamic sensorimotor interactions in locomotion. *Physiol Rev* 86: 89–154, 2006.

Schaal S. Dynamic movement primitives-a framework for motor control in humans and humanoid robotics. In: *Adaptive motion of animals and machines*. Springer, 2006. p. 261–280.

Schaal S, Sternad D, Atkeson CG. One-handed juggling: A dynamical approach to a rhythmic movement task. *J Mot Behav* 28: 165–183, 1996.

Schmidt R, Bienvenu M, Fitzpatrick P, Amazeen P. A comparison of intra-and interpersonal interlimb coordination: Coordination breakdowns and coupling strength. *Journal of Experimental Psychology: Human Perception and Performance* 24: 884, 1998.

Schmidt R, Richardson MJ, Arsenault C, Galantucci B. Visual tracking and entrainment to an environmental rhythm. *Journal of Experimental Psychology: Human Perception and Performance* 33: 860, 2007.

Siegler IA, Bardy BG, Warren WH. Passive vs. active control of rhythmic ball bouncing: the role of visual information. *J Exp Psychol Hum Percept Perform* 36: 729–50, 2010.

Siegler IA, Bazile C, Warren W. Mixed control for perception and action: timing and error correction in rhythmic ball-bouncing. *Exp Brain Res* 226: 603–615, 2013.

Sternad D, Duarte M, Katsumata H, Schaal S. Bouncing a ball: tuning into dynamic stability. *J Exp Psychol Hum Percept Perform* 27: 1163, 2001.

Taga G. A model of the neuro-musculo-skeletal system for human locomotion. *Biol Cybern* 73: 97–111, 1995.

Van Der Steen MC, Keller PE. The adaptation and anticipation model (adam) of sensorimotor synchronization. *Frontiers in human neuroscience* 7: 253, 2013.

Vincent TL, Mees AI. Controlling a bouncing ball. *Int J of Bifurcation and Chaos* 10: 579–592, 2000.

Warren WH. The dynamics of perception and action. *Psychol Rev* 113: 358–389, 2006.

Wei K, Dijkstra T, Sternad D. Passive stabiliy and variability: indicators for passive stability and active control in a rhythmic task. *J Neurophysiol* 98: 2633–2646, 2007.

Wei K, Dijkstra TMH, Sternad D. Stability and variability: Indicators for passive stability and active control in a rhythmic task. *J Neurophysiol* 99: 3027–3041, 2008.

Williamson M. Designing rhythmic motions using neural oscillators. *Proc IEEE/RSJ Int Conf on Intelligent Robots and Systems (IROS)* 1: 494–500, 1999.

Wimmers RH, Beek PJ, van Wieringen PC. Phase transitions in rhythmic tracking movements: A case of unilateral coupling. *Human Movement Science* 11: 217–226, 1992.

Yagoubi M, Sandou G. Particle Swarm Optimization for the design of H∞ static output feedbacks. *Proc IFAC World Congr* , 2011.

Zehr EP, Carroll TJ, Chua R, Collins DF, Frigon A, Haridas C, Hundza SR, Thompson AK. Possible contributions of CPG activity to the control of rhythmic human arm movement. *Can J Physiol Pharmacol* 82: 556–568, 2004.

Zhang D, Zhu X, Poignet P. Coupling of central and peripheral mechanism on tremor. *Proc IEEE/EMBS Int Conf Neural Engineering* p. 649–652, 2009.

Zhao H, Warren WH. On-line and model-based approaches to the visual control of action. *Vision research* 110: 190–202, 2015.

List of Figures

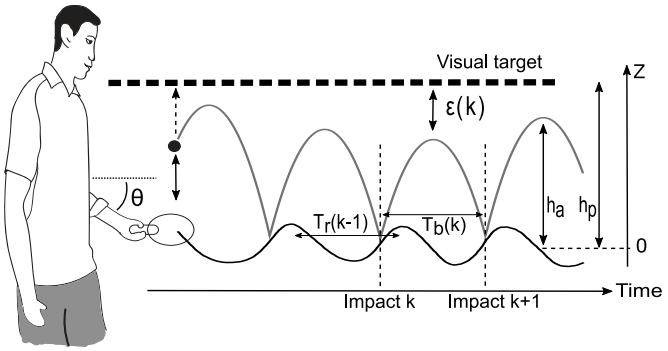

FIG. 1. The ball-bouncing task (see Section 1.1.1 for legends).

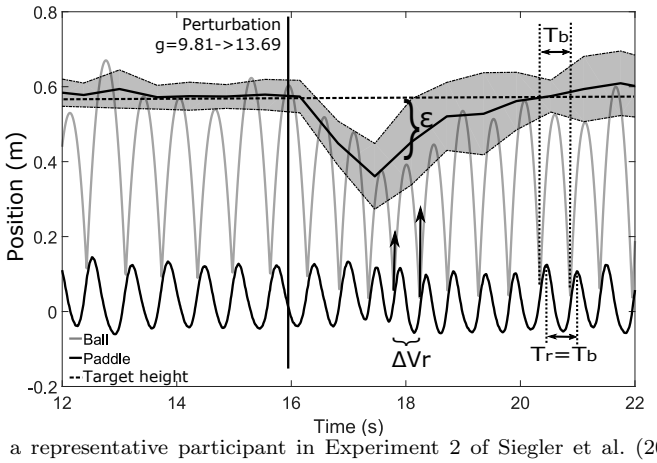

FIG. 2. Example of perturbed trial from a representative participant in Experiment 2 of Siegler et al. (2010). The 13 participants' bounce error standard deviation is represented by the shaded region superimposed on the figure. The participants' mean bounce error is represented by the solid dark gray line centered on this shaded region.

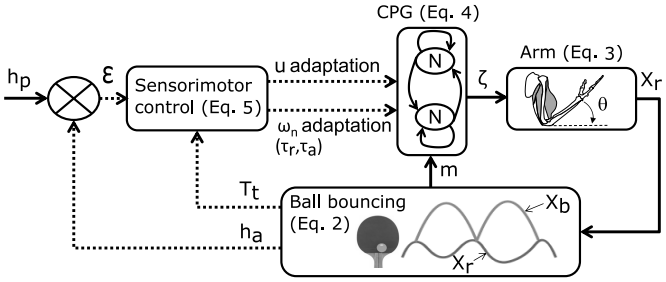

FIG. 3. Sensorimotor control model of the ball-bouncing task.

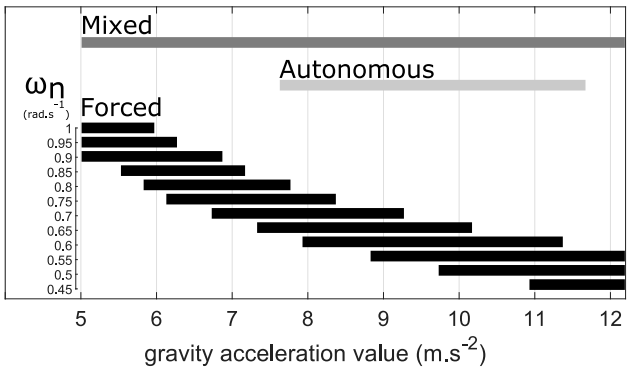

FIG. 4. Intervals of gravity acceleration values leading to stable bouncing for the three oscillator operating modes. For forced mode, different oscillator natural frequencies are considered.

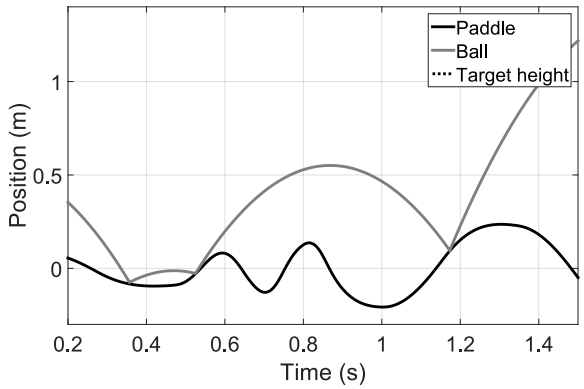

FIG. 5. Unrealistic behavior produced by autonomous oscillation mode: after a perturbation or a bad bounce, the paddle completed two cycles meanwhile the ball barely reached its apex.

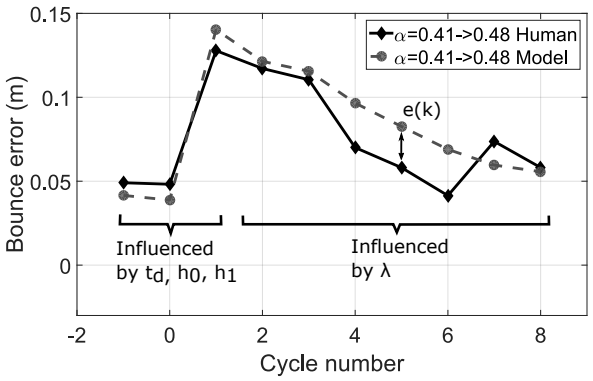

FIG. 6. Example of bounce errors series used for limit cycle and transient-state tuning by minimization of MSE(e).

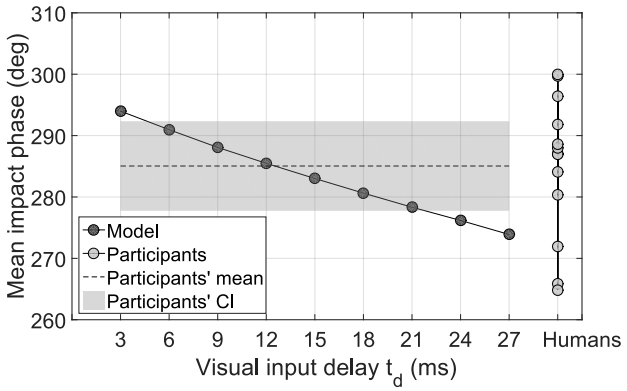

FIG. 7. Influence of t_d on the impact phase, for $h_0 = 96.54$, $h_1 = 0.610$ and $\lambda = -3.4$, compared to the impact phase of the 13 participants. The environmental conditions are: $g = 9.81, \alpha = 0.41$.

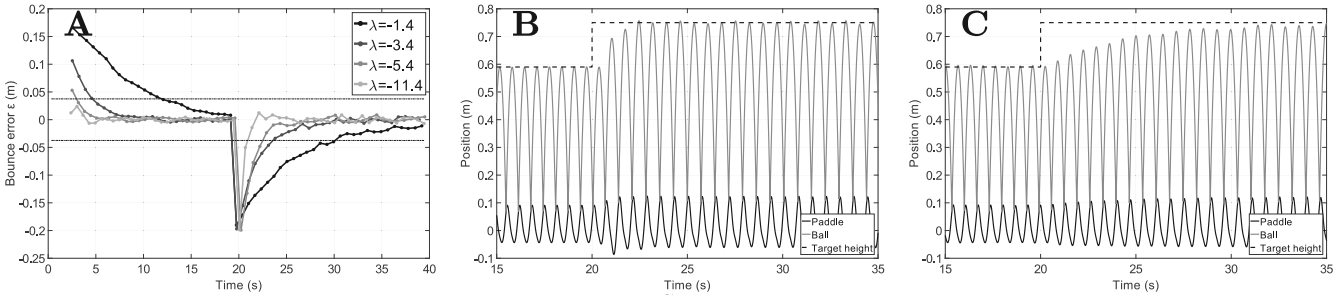

FIG. 8. A: Influence of λ on system response time after a target height change (h_p : $0.59 \rightarrow 0.75m$). B: With a high absolute value of λ, the convergence to target is fast. Here $\lambda = -10$. C: With a small absolute value of λ, the convergence is slower than in B. Here $\lambda = -2$. Simulations for the environmental conditions $g = 9.81,\ \alpha = 0.48$.

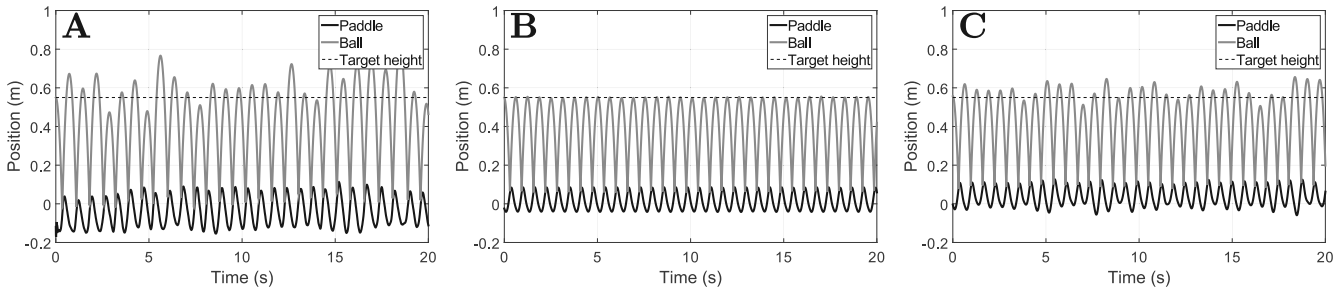

FIG. 9. A: Example of human ball-bouncing. B: Example of ball-bouncing simulation without noise ($\lambda = -3.4,\ S_1 = S_2 = S_3 = 0$). C: Example of ball-bouncing simulation with motor noise ($\lambda = -3.4,\ S_1 = 0.946,\ S_2 = S_3 = 0$).

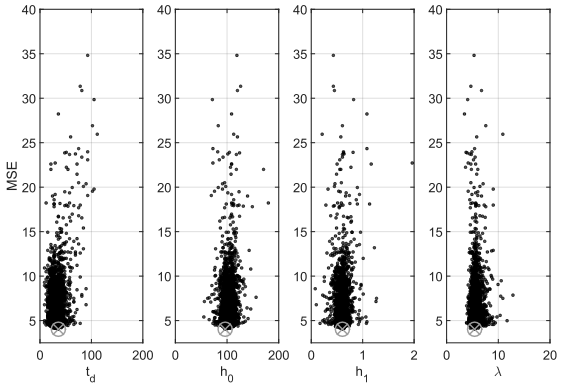

FIG. 10. Convergence of the PSO for limit cycle shaping. All the values tested are indicated with black dots. The chosen parameter set is indicated by a gray marker $\otimes$.

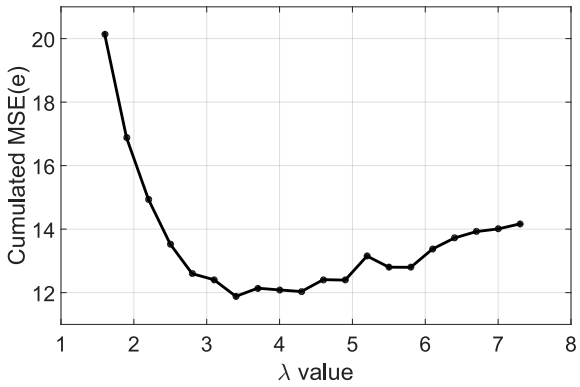

FIG. 11. Cumulated MSE between the participants and model bounce error series from the tuning conditions, as a function of λ.

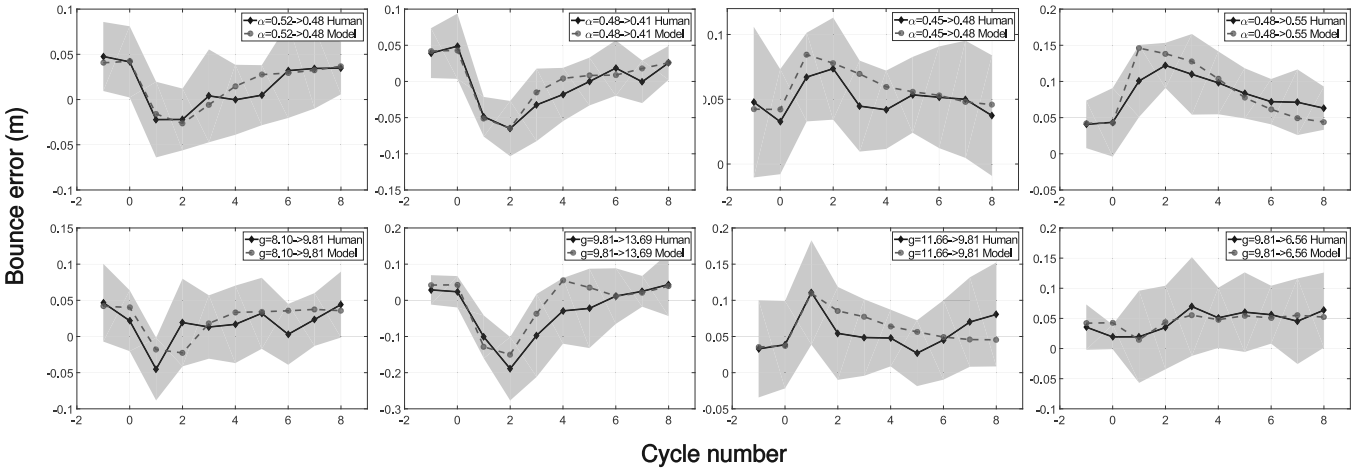

FIG. 12. Bounce error for each cycle around perturbation of **tuning trials** of session A (first row) and session G (second row). Perturbation occurs at the beginning of cycle 1. The 13 participants' mean bounce error is represented by a solid line with diamond markers. The participants' bounce error standard deviation is represented by the shaded region.The model bounce errors are represented by the dashed line with round markers.

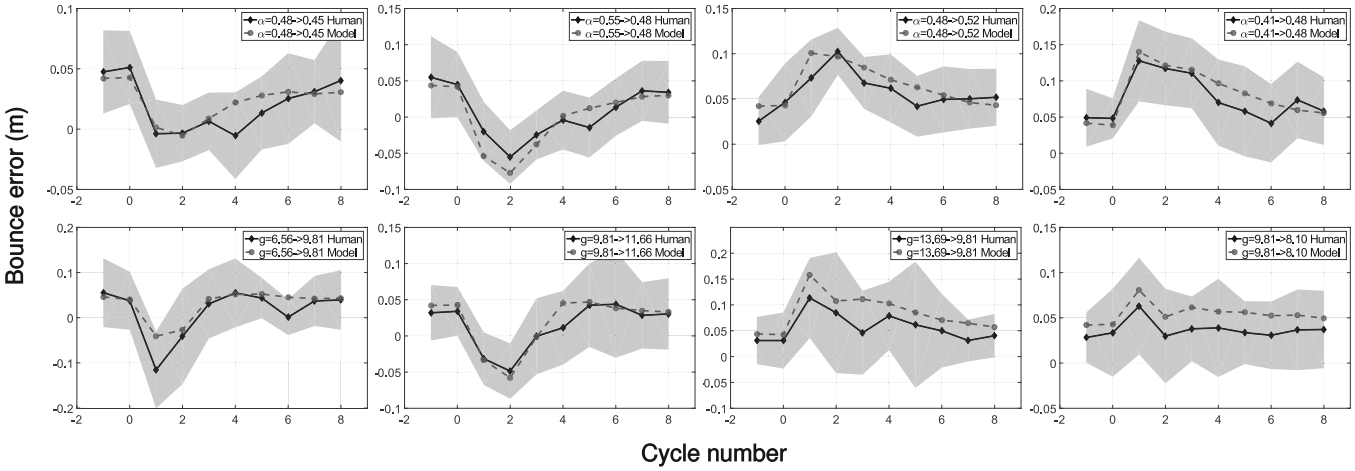

FIG. 13. Bounce error for each cycle around perturbation of **validation trials** of session A (first row) and session G (second row). The perturbation occurs at the beginning of cycle 1. The 13 participants' mean bounce error is represented by a solid line with diamond markers. The participants' bounce error standard deviation is represented by the shaded region.The model bounce errors are represented by the dashed line with round markers.

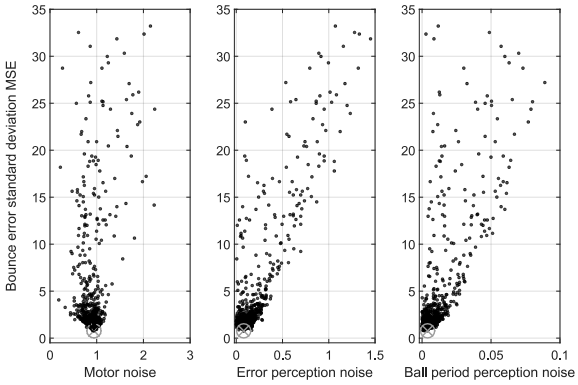

FIG. 14. Convergence of the PSO for noises strengths tuning. The black dots indicate the tested values that led to stable bouncing. The chosen parameter set is indicated by a gray marker ⊗.

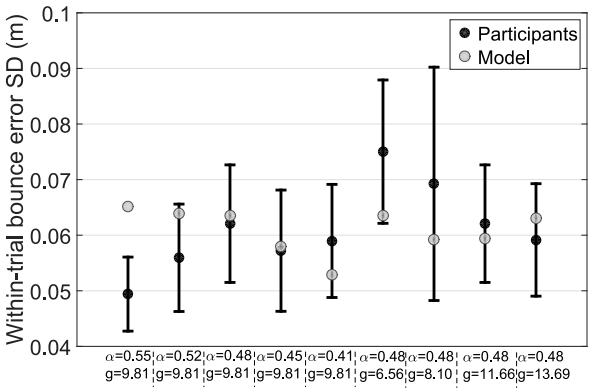

FIG. 15. Mean of within-trial bounce error standard deviations (black circles: 13 participants; gray circles: 13 model simulations). The bars represent CI of participants' mean bounce error standard deviation (with $\lambda = -3.4,\ t_d = 36\,ms,\ h_0 = 96.54,\ h_1 = 0.610,\ S_1 = 0.946,\ S_2 = 0.083,\ S_3 = 0.004$).

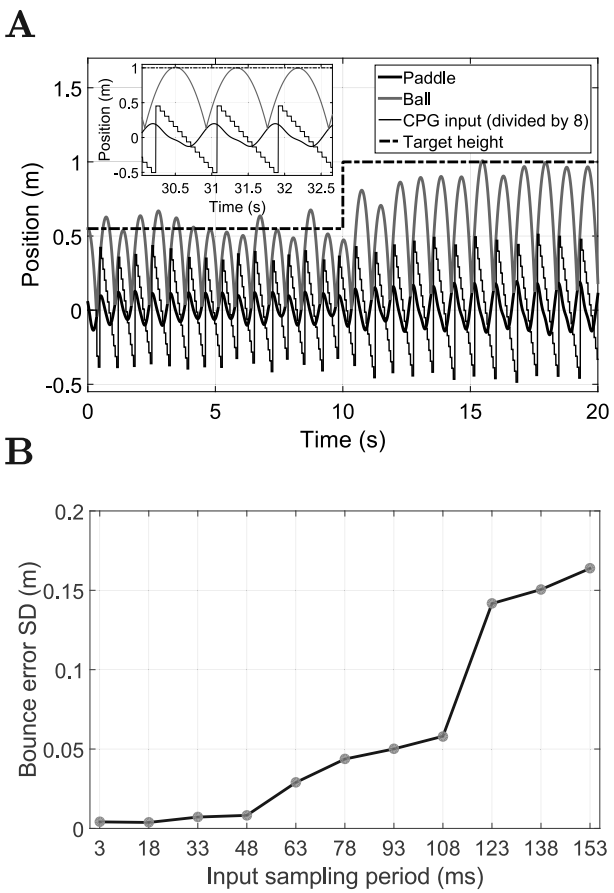

FIG. 16. A: Ball-bouncing task for a discrete CPG input (discrete perception of delayed ball velocity) with an input sampling period equal to 60 ms. B: Evolution of bounce error standard deviation as a function of the input sampling period, for simulation lasting 30 s with $g = 9.81$ and $\alpha = 0.48$). Both simulations are run without noise ($S_1 = S_2 = S_3 = 0$).